ACS APPLIED MATERIALS & INTERFACES

Research Article

www.acsami.org

Multidentate Polyethylene Glycol Modified Gold Nanorods for in Vivo Near-Infrared Photothermal Cancer Therapy

Xiangsheng Liu, Nan Huang, Huan Li, Haibo Wang, Qiao Jin, and Jian Ji*

MOE Key Laboratory of Macromolecular Synthesis and Functionalization, Department of Polymer Science and Engineering, Zhejiang University, Hangzhou 310027, China

Supporting Information

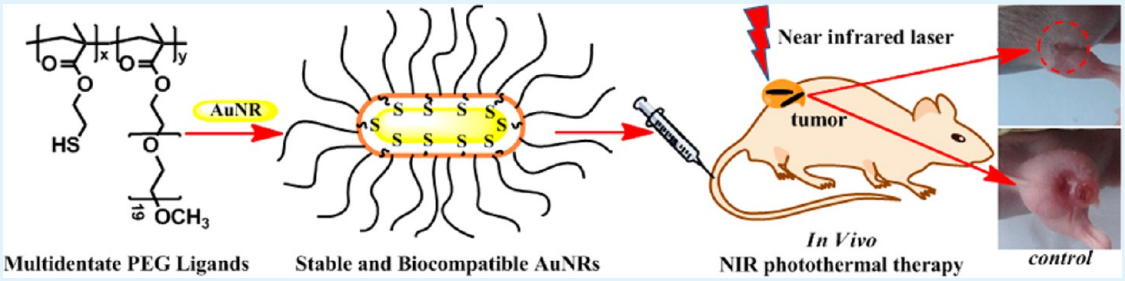

ABSTRACT: Gold nanorods (AuNRs), because of their strong absorption of near-infrared (NIR) light, are very suitable for in vivo photothermal therapy of cancer. However, appropriate surface modification must be performed on AuNRs before their in vivo application because of the high toxicity of their original stabilizer cetyltrimethylammonium bromide. Multidentate ligands have attracted a lot of attention for modification of inorganic nanoparticles (NPs) because of their high ligand affinity and multifunctionality, while the therapeutic effect of multidentate ligands modified NPs in vivo remains unexplored. Here, we modified AuNRs with a polythiol PEG-based copolymer. The multidentate PEG coated AuNRs (AuNR-PTPEGm950) showed good stabilities in high saline condition and wide pH range. And they had much stronger resistance to ligand competition of dithiothreitol (DTT) than AuNRs coated by monothiol-anchored PEG. The AuNR-PTPEGm950 had very low cytotoxicity and showed high efficacy for the ablation of cancer cells in vitro. Moreover, the AuNR-PTPEGm950 showed good stability in serum, and they had a long circulation time in blood that led to a high accumulation in tumors after intravenous injection. In vivo photothermal therapy showed that tumors were completely cured without reoccurrence by one-time irradiation of NIR laser after a single injection of these multidentate PEG modified AuNRs.

KEYWORDS: *gold nanorods, multidentate polyethylene glycol, surface modification, tumor accumulation, cancer NIR photothermal therapy*

1. INTRODUCTION

Inorganic nanoparticles (NPs), because of their unique physicochemical properties, provide promising tools in cancer diagnosis and therapy including drug/gene delivery, biosensing, bioimaging, and photodynamic/photothermal therapy.[1−6] However, realizing their functions successfully in complex biological systems is not easy.[4,7,8] For in vivo application, the NPs should first have good colloidal stability and biocompatibility. Moreover, to obtain high therapeutic efficacy, the NPs need to have targeting ability to the tumor site. It is well known that NPs, because of their size effect, have more chance to arrive at tumor tissues than normal tissues by taking advantage of enhanced permeability and retention (EPR) effect in solid tumors that have defective vascular architecture with high permeability and impaired lymphatic drainage system.[9,10] The EPR effect is known as the "golden standard" for drug design to tumor therapy, but it requires the systemically administered NPs to remain in blood circulation for a long time to have enough chance to accumulate in tumors through the leaky vasculature.[9,10] Nanoparticles that aggregate or nonspecifically adsorb proteins in blood will be easily cleared by the reticuloendothelial system (RES) or mononuclear phagocyte system (MPS), which usually results in a short blood circulation time,[9−12] which will greatly reduce the efficiency of tumor targeting.

To fabricate stable, biocompatible, and long-circulating NPs, suitable surface modification is one of the most effective ways.[13−16] Ideally, a desirable coating material should first have high affinity to the NP surface and also provide NPs with chemical functionality, good colloidal stability, biocompatibility, and antifouling property.[14] Recently, multidentate polymer ligands have attracted great attention because of their ability for enhancing the affinity of ligands to inorganic NPs and endowing the modified NPs with multifunctional property.[17−26] Polyethylene glycol (PEG)[20,21,24,26,27] and zwitterionic groups such as phosphorylcholine[22,25] and sulfobe-

Received: January 10, 2014
Accepted: March 27, 2014
Published: March 27, 2014

   dx.doi.org/10.1021/am5001823 | ACS Appl. Mater. Interfaces 2014, 6, 5657−5668

Scheme 1. Schematic Representation of Surface Modification of CTAB Capped AuNRs with Polythiol PEG Based Copolymer for in Vivo Photothermal Therapy (Not to Scale)

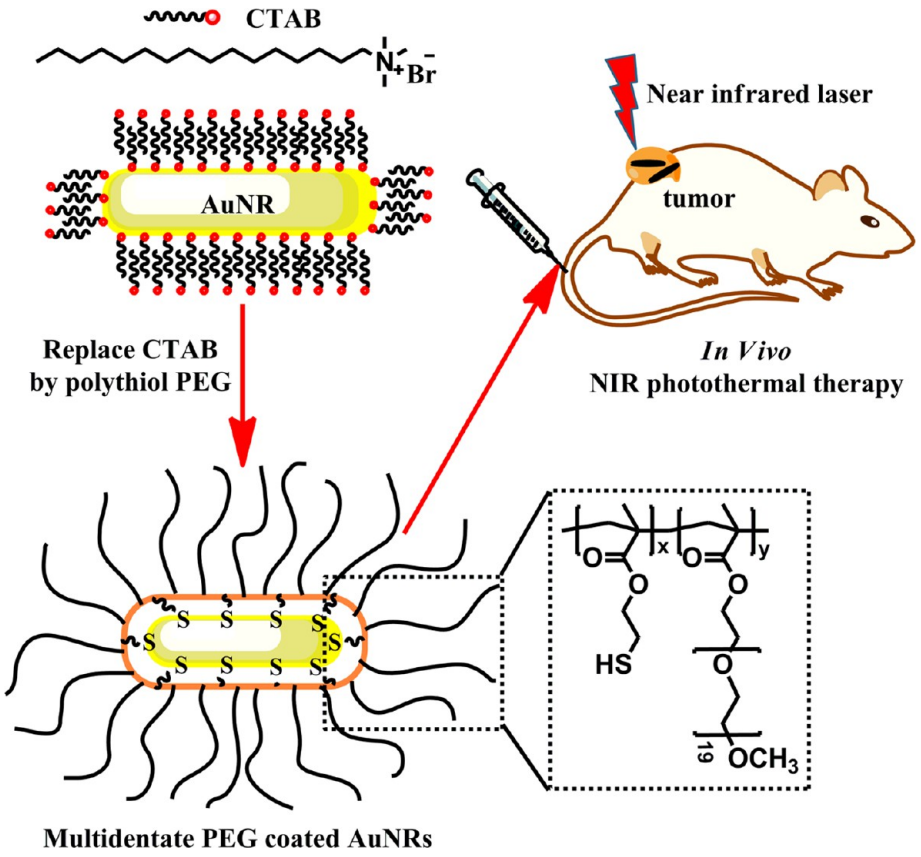

taine,[23,28] because of their excellent hydrophilicity and antifouling ability, have been designed into multidentate ligands that have been demonstrated to endow NPs with good stability, biocompatibility, and nonfouling property both in vitro[20−22,24,25,28] and in vivo.[26,27] Although the great potential of using the multidentate ligands in nanomedicine is promised by their fascinating properties, there is still no report that demonstrates the therapeutic efficacy of multidentate ligand coated NPs in vivo.

Gold nanoparticles with unique surface plasmon resonance (SPR) can strongly absorb light and efficiently convert the light into localized heat.[29,30] The heat can be utilized to selectively ablate cancer cells, which is known as plasmonic photothermal therapy (PPTT).[30] It provides an attractive method for treating solid tumors in a minimally invasive manner and may have several advantages, such as fast recovery, fewer complications, and shorter hospital stay.[31] In particular, for in vivo therapy of tumors under skin and deeply seated within tissue, near-infrared (NIR, ~650-900 nm) light which has been shown to have a deep penetration in tissues up to 4−10 cm is strongly desired.[32] The NIR light used in this manner provides deep-tissue penetration with high spatial precision without damaging normal biological tissues due to minimal absorption by the hemoglobin and water molecules in normal tissues in this spectral region.[31,32] Encouragingly, many gold nanostructures are designed successfully, including silica/gold nanoshells,[33] gold nanorods,[34] gold nanocages,[35] hollow gold nanospheres,[36] and nanomicelle-based gold nanoshells,[37] that absorb light strongly within the tissue-transparent NIR region. Among them, gold nanorods (AuNRs) have attracted much interest for biomedical application because of their advantages like efficient large-scale synthesis, high optical absorption coefficients in the NIR region, and precisely tunable absorption range of light by adjusting their aspect ratio.[34,38,39] Especially, AuNRs have been demonstrated to be one of the most efficient exogenous agents for NIR photothermal cancer therapy, which showed high efficacy in ablation of cancer cells in vitro[40−42] or tumors in vivo.[31,43,44] Co-delivery of anticancer drugs carried by AuNRs showed the combined photothermal-chemotherapy with enhanced antitumor effect.[45−47] Moreover, AuNRs also showed great promise for cancer diagnostics such as X-ray CT imaging, photoacoustic imaging, and surface-enhanced Raman imaging in living mice.[44,48,49] Despite these advantages, the synthesized AuNRs capped with excess positive surfactant cetyltrimethylammonium bromide (CTAB) are very toxic to cells and unstable in serum which is not suitable for direct clinical application.[44,50] It was also reported that the CTAB-stabilized AuNRs were rapidly cleared out from blood at 0.5 h after intravenous injection because of the opsonization and fast uptake by RES.[51] Therefore, a biocompatible and antifouling coating is needed to cover AuNRs by certain surface modification before clinic use. PEGylation is the most applied strategy to modify the AuNRs, which makes the AuNRs obtain good stability, biocompatibility, long blood-circulation time, and effective tumor accumulation.[41,43,44,51]

Recently, we developed PEG-based multidentate ligands to modify gold nanospheres and studied the effect of the ligand's composition on NP's fate in vivo.[27] It showed that the copolymer with about 1:2 ratio of mercapto groups to PEG segments could well stabilize the gold nanospheres with high

dx.doi.org/10.1021/am5001823 | ACS Appl. Mater. Interfaces 2014, 6, 5657−5668

tumor accumulation. The polythiol PEG-based ligand (PTPEGm950) showed great promise for modifying other metal nanoparticles because of the strong reactivity of thiols. Therefore, in this study, we applied the multidentate PEG copolymer to modify the AuNRs (Scheme 1) and used the coated AuNRs as photothermal agents for cancer therapy. The modified AuNRs showed good stability, low cytotoxicity, and effective photothermal ablation of cancer cells in vitro. Most of all, the multidentate ligand modified AuNRs exhibited long blood circulation time and high tumor accumulation in vivo and led to a very impressive therapeutic effect in nude mice bearing tumors by treating with a safe NIR laser.

2. EXPERIMENTAL SECTION

2.1. Materials. Cetyltrimethylammonium bromide (CTAB) was purchased from Aladdin Reagents Inc. Dithiothreitol (DTT) was purchased from Sangon Biotech (Shanghai) Co., Ltd. Hydrogen tetrachloroaurate hydrate ($HAuCl_4{\cdot}4H_2O$), ascorbic acid (AA), sodium borohydride ($NaBH_4$), silver nitrate ($AgNO_3$), and other common regents were purchased from Sinopharm Chemical Reagent Co., Ltd. 2,2′-Dithiodiethanol, 3-[4,5-dimethylthiazol-2-yl]-2,5-diphenyltetrazolium bromide (MTT), and fluorescein diacetate (FDA) were purchased from Sigma-Aldrich. All reagents for the cell culture were directly used after being purchased from Gibco or Dawen Biotech (Hangzhou) Co., Ltd. All water was distilled and subsequently purified to Millipore Milli-Q quality.

2.2. Synthesis of CTAB and PTPEGm950 Coated AuNRs. The synthesis of AuNRs was referenced to the methods by El-Sayed et al.,[52] Murphy et al.,[53] and Zubarev et al.[54] with slight modifications. First, the growth solution was prepared in advance by added 0.35 mL of 78.8 mM AA to 50 mL solution of 100 mM CTAB, 0.5 mM $HAuCl_4$, and 0.1 mM $AgNO_3$, which resulted in a colorless solution. Then the gold seeds were prepared by adding 0.6 mL of ice solution of 10 mM $NaBH_4$ into a 10 mL solution of 100 mM CTAB and 0.25 mM $HAuCl_4$ with vigorous stirring, which resulted in the formation of a brownish yellow solution. Vigorous stirring of the seed solution was continued for 10 min. To prepare AuNRs with a longitudinal absorption band around 800 nm, 1.5 mL of the aged seed solution was added to the growth solution. The mixed solution was shaken for 2−5 min and then kept still overnight at 27 °C to finally generate CTAB capped AuNRs.

For further surface modification, the synthesized AuNRs were first centrifuged twice at 16 000 rpm for 10 min to remove the excess CTAB, and then the purified AuNRs were redispersed in the same amount water. PTPEGm950 was prepared as previously reported, and the ratio of mercapto groups to PEG segments was ∼1:2.[27] There are about 6 thiol groups and 14 PEG chains per polymer as estimated from for ^{1}H NMR and GPC results.[27] The polymer protected AuNRs were obtained by exchange of CTAB molecules on AuNRs with thiolated PTPEGm950. Briefly, 10 mg of PMTPEGm950 was dissolved in 10 mL of water, which then was added into the purified AuNRs solution (50 mL). After the mixture was stirred at room temperature for 24 h, the modified AuNRs were purified by centrifugation twice at 16 000 rpm for 15 min and then dispersed in PBS and filtered through syringe filters with cellulose acetate membranes with a pore size of 0.45 μm. The AuNR concentration was analyzed by ICP-MS (Thermo Elemental Corporation of USA, X series II).

2.3. Stability of AuNRs. The stabilities of AuNR-PTPEGm950 at various situations were tested by UV−vis spectra collected within a range of 400−900 nm. To determine AuNPs stability with respect to various conditions, the AuNRs in water were added to test solutions in a 1:1 volume ratio, including 10 mM phosphate buffered solution (PB solution) with 2-fold desired NaCl concentrations, 2-fold physiological phosphate buffered saline (PBS, 8 g of NaCl, 0.2 g of KCl, 2.9 g of $Na_2HPO_4{\cdot}12H_2O$, 0.2 g of KH_2PO_4 in 1000 mL of water, pH 7.4), and PB (10 mM) solutions at pH 1−13. The spectra were recorded 10 min after the conditions of the AuNR solution were adjusted. To determine the stability of biological complex media, AuNRs were added to 100% fetal bovine serum (FBS) in a 1:10 volume ratio and the solution was checked after 24 h by UV−vis spectroscopy to see if any aggregation had occurred.

2.4. DTT Competition Tests. The DTT competition tests were performed according to the reference but with slight modification.[20] Briefly, the amount of water and AuNR stock solution added to each cuvette was calculated to yield an optical density at the longitudinal absorption band around 800 nm of ∼0.35−0.4 at a final solution volume of 200 μL. First, DTT (1.5 M) was added to a solution of NaCl (4 M) in the quartz cuvette and thoroughly mixed. The appropriate volumes of AuNR stock solution and water were added to make the final desired concentrations of AuNRs, DTT, and NaCl, mixed for 30 s, and a series of absorption spectra were collected at various time intervals to track changes in the spectra.

2.5. Characterization. Optical absorption spectra were obtained using a UV−vis Shimadzu UV-2505 spectrometer with 1 cm path length quartz cuvettes. The morphology and size of the NRs were determined using transmission electron microscopy (TEM) performed with a JEM-1230EX TEM instrument operating at 80 kV in bright field mode. FT-IR analysis was performed with a Bruker Vector2 spectrometer. The hydrodynamic size and ζ potential of the AuNRs were measured using dynamic light scattering (DLS; the hydrodynamic sizes obtained from DLS of anisotropic AuNRs are not exact because the data were fitted to a spherical model and here they are only used to present the tendency of size change for the AuNRs after surface modification). Measurements were performed using a Zetasizer Nano-ZS from Malvern Instruments equipped with a He−Ne laser with a wavelength of 633 nm at 25 °C using a detection angle of 173°.

2.6. Cell Culture. Human umbilical vein endothelial cell line (HUVEC), human oral epidermoid carcinoma cell line (KB), and human hepatocarcinoma cell line (HepG2) were purchased from China Center for Typical Culture Collection. HUVEC and KB cells were cultured with RPMI 1640 medium, and HepG2 cells were cultured with Dulbecco's modified Eagle medium (DMEM). All cells were cultured in the medium supplemented with 10 % FBS, 100 U/mL penicillin, and 100 mg/mL streptomycin and cultured at 37 °C in a 5% CO_2 humidified environment.

2.7. Cytotoxicity Assay. Cytotoxicity of AuNRs was performed by standard MTT assay as previously reported.[25] To determine the relative cell viability by MTT assay, cells were plated at a density of 5×10^3 cells per well in a 96-well plate and cultured for 24 h. The medium was replaced with fresh medium containing the AuNRs of varying concentrations (the Au atomic concentration was determined by ICP-MS). Cells cultured in nanoparticle-free media were used as a control. After treatment for 24 h, the wells were washed with PBS, the medium was replaced with 100 μL of fresh medium, 20 μL of MTT (5 mg mL^{-1}) was added to each well, and the cells were further cultured at 37 °C for 4 h. The dark blue formazan crystals generated by the mitochondria dehydrogenase in live cells were dissolved with 150 μL of dimethyl sulfoxide to measure the absorbance at 570 nm by a microplate reader (model 550, Bio Rad). The relative cell viability (%) is [(the absorption of treated well)/(the absorption of control well)] × 100.

2.8. NIR Photothermal Assay in Vitro. HepG2 cells were plated in a 96-well plate and cultivated to near 100% confluence. For laser irradiation, the medium was carefully removed and an amount of 20 μL of fresh medium containing AuNRs at different concentrations was added. Then the cells were irradiated using a continuous-wave (CW) diode laser at 808 nm with a ∼1 mm focused spot size at a power of 400 mW for 1 min. The cells irradiated under the same condition but without AuNRs were chosen as control. Cell viability was confirmed by staining the cells with FDA. The live cells can manufacture fluorescein from FDA by esterase inside cells, while the dead cells cannot. The CW diode laser with wavelength of 808 nm was purchased from Hi-Tech Optoelectronics Co., Ltd.

2.9. Animals. Animal experiments were performed according to Guidelines of Animal Care and Use Committee, Zhejiang University. Healthy male Institute of Cancer Research (ICR) mice and male

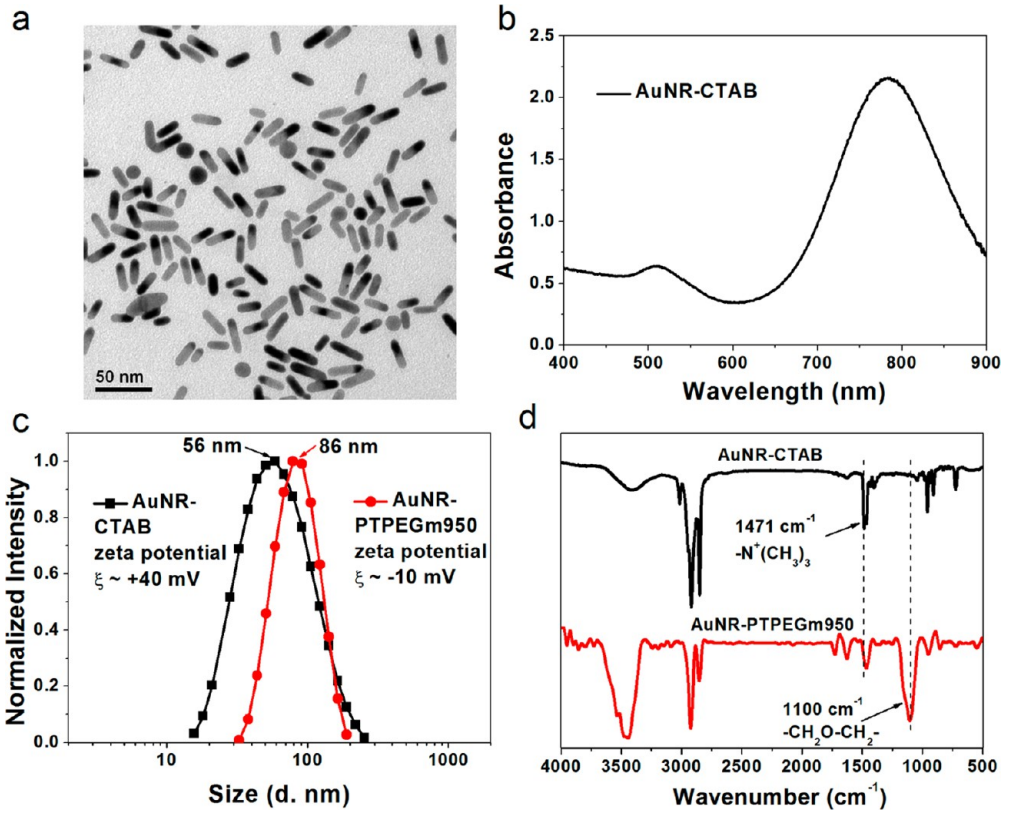

Figure 1. (a) TEM image and (b) absorption spectrum of AuNRs. (c) Hydrodynamic sizes and ζ potential of AuNRs before and after surface modification measured by DLS. The hydrodynamic sizes obtained from DLS of anisotropic AuNRs are not exact because the data were fitted to a spherical model and here they are only used to present the tendency of size change for the AuNRs after surface modification. (d) FT-IR spectra of CTAB and PTPEGm950 coated AuNRs.

BALB/c nude mice were purchased from the animal center of Zhejiang Academy of Medical Sciences.

2.10. Blood Circulation and Biodistribution of AuNR-PTPEGm950. AuNRs given in 0.1 mL solution with 100 μg of Au were injected via the tail vein in each mouse (male ICR mice, 18−22 g). Blood circulation analysis was performed by measuring the remaining gold content from blood taken after injection at different times. Blood samples were collected at 5 min, and 1, 3, 6, 12, and 24 h postinjection (pi), and the total blood weight was estimated to be ~7% of body weight. Biodistribution analysis was performed by measuring the gold content in main organs including the liver, kidneys, spleen, heart, and lung, which was collected in 1 day pi. The gold content was analyzed by ICP-MS.

2.11. Histology. For histology, major organs (liver, kidneys, and spleen) were harvested from those mice after injection for 24 h. Organs were fixed in 3.7% neutral buffered formalin, processed routinely into paraffin, sectioned into 4 μm, and stained with hematoxylin and eosin (H&E). The histology was performed in a blind fashion by professional personnel in the medical college of Zhejiang University. The samples were examined by microscope (Olympus BX61 inverted microscope) in bright field.

2.12. Tumor Xenografts. KB cells (2×10^6) in 0.1 mL of PBS were injected subcutaneously into the rear flank area of male nude BALB/c mice of weight 16−18 g. Tumor dimensions (length and width) were measured using a caliper. The tumor volume was calculated as length × width^2/2 (mm^3). Tumors were allowed to grow to ~100 mm^3 before experimentation.

2.13. Tumor Accumulation. AuNRs given in 0.1 mL of PBS with 100 μg or 50 μg of Au were injected via the tail vein in each tumor-bearing mouse. The mice were sacrificed at 24 h postinjection, and tumors were collected for measuring their Au content by ICP-MS.

2.14. ICP-MS Measurement. Organs and tumors were washed in PBS buffer, weighted, and lyophilized for 1 day. Blood was lyophilized directly. The dried tissues and blood were mashed and dissolved in aqua regia for 24 h. Then the aqua regia was diluted and the precipitated tissue debris was removed by centrifugation at 10 000 rpm for 5 min. The Au content in the supernatant was detected by ICP-MS.

2.15. NIR Photothermal Assay in Vivo. For safety test of laser irradiation on normal tissues, the healthy mouse thigh was irradiated by a CW diode laser at 808 nm with a ~6 mm focused spot size at a power of 1.56 W for 5 min or a power of 3.9 W for 2 min. For tumor ablation study, AuNR-PTPEGm950 given in 0.1 mL of PBS with 50 μg of Au, 100 μg of Au or pure PBS without AuNRs as control was injected via the tail vein in each tumor-bearing mouse. After 24 h, the tumors were irradiated by the 808 nm laser at a power of 1.56 W for 2.5 or 5 min. Mice injected with PBS or 100 μg of AuNRs but without irradiation were also conducted as controls. The tumor growth of all these treated groups was monitored by taking photos of tumors up to 16 days after treatment. The CW laser (MDL-N-808nm) with wavelength of 808 nm was purchased from Changchun New Industries Optoelectronics Tech. Co., Ltd.

3. RESULTS AND DISCUSSION

3.1. Preparation and Characterization of PTPEGm950 Modified AuNRs. AuNRs were synthesized according to the seed-mediated growth method with slight modification.[52−54] The prepared AuNRs had an aspect ratio of ~3.7, which averaged 28 nm in length and 7.5 nm in width (Figure 1a). They showed a longitudinal absorption band at around 785 nm which overlapped well with the NIR region (Figure 1b). After modification with polythiol PEG ligand (PTPEGm950), the hydrodynamic size obtained by DLS measurement of modified AuNRs (~86 nm, AuNR-PTPEGm950) was increased compared to the CTAB capped AuNRs (~56 nm, AuNR-

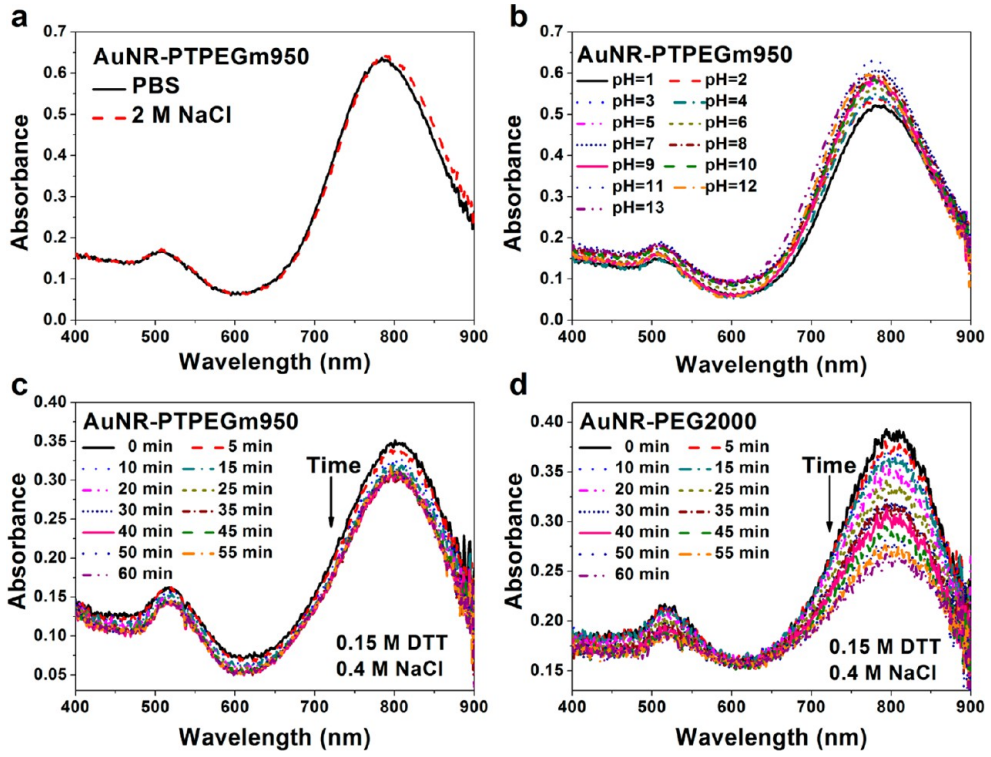

Figure 2. UV−vis spectra of AuNR-PTPEGm950 incubated in (a) physiological phosphate buffered saline (PBS) and solution with 2 M NaCl and (b) phosphate buffered solutions with various pH values from 1 to 13. Time-dependent absorption spectra of AuNRs capped with (c) PTPEGm950 and (d) HS-PEG2000 from 0 to 60 min in the presence of 0.15 M DTT and 0.4 M NaCl.

CTAB) because of the polymer layers covered on the AuNRs (Figure 1c). The ζ potential of AuNRs was changed from strongly positive (∼+40 mV) to slightly negative (∼−10 mV) after modification, which indicated good replacement of CTAB ligands on NRs. FT-IR analysis also confirmed the surface conjugation of AuNRs with PEG-based polymethacrylate, where the strong band at ∼1471 cm^{-1} (ascribed to trimethylammonium group of CTAB) disappeared and a new strong band at ∼1050 cm^{-1} (ascribed to ether bonds of PEG chains) was measured in the spectrum of AuNR-PTPEGm950 (Figure 1d).

3.2. Colloidal Stability and Ligand Affinity of PEG Coated AuNRs. The stabilities of AuNR-PTPEGM950 samples were investigated under various conditions, including physiological phosphate buffered saline (PBS), saline solutions with high NaCl concentration (2000 mM), and solutions of different pH. The UV−vis spectra of AuNR-PTPEGM950 in PBS and 2 M NaCl kept good shape as prepared, with a typical high longitudinal plasmon peak at ∼785 nm and a low transverse plasmon peak at ∼510 nm (Figure 2a). Under pH range from 1 to 13, the UV−vis spectra of AuNR-PTPEGM950 all kept a similar shape, which indicated no detectable aggregation of AuNRs had happened (Figure 2b). However, AuNR-CTAB aggregated seriously in PBS and alkaline PB solution (Figure S1 in Supporting Information). These results showed that the multidentate PEG ligand could stabilize AuNRs with strong resistance to high ionic strength and wide pH conditions that could be attributed to the effects of steric exclusion, surface hydration, and pH-insusceptibility of PEG chains.

One main advantage of multidentate ligands is their strong affinity to NPs, which is expected to keep stable coating on NPs under competitive environment. For thiol ligands, their linkage to metal surface could be affected by other types of thiols in the environment such as glutathione or proteins with mercapto groups in biological systems.[20] The ligand affinity of the multidentate ligands to AuNRs can be tested in the presence of strong competition by a dithiol reducing agent DTT.[20] At high concentrations, DTT can displace weakly to modestly bound ligands from the surface of AuNRs, inducing progressive aggregation. This process can be further accelerated in the presence of excess NaCl. We compared the stability of polythiol PEG coated AuNRs with monothiol-anchored HS-PEG2000 coated AuNRs (AuNR-PEG2000) under DTT competition condition. Figure 2c showed the time evolution of the absorption spectra collected for AuNR-PTPEGm950 in aqueous solutions containing 0.15 M DTT (large excess) and 0.4 M NaCl, and no significant shape change of the spectra was observed after 60 min. However, the spectra of AuNR-PEG2000 changed remarkably under the same conditions with an obvious decreased absorption at the longitudinal band range (Figure 2d). It demonstrated that the AuNRs capped with the multidentate PTPEGm950 have much stronger resistance to competition of thiol agents than the monothiol ligand modified AuNRs. Combined with the superstabilities of the previous PTPEGm950 modified gold nanospheres, these results strongly suggest that the polythiol PEG ligand could be widely used to stabilize various types of gold nanoparticles with improved stability which should improve their performance in certain bioapplications, where the ability to resist thiol-rich, high electrolyte concentration, and wide pHs is highly desirable.

3.3. Cytotoxicity of Multidentate PEG Coated AuNRs. Among the various gold nanostructures, the cytotoxicity of AuNRs is special because of the excess toxic CTAB used in the synthetic process. Much of the cytotoxicity of AuNRs resulted from the residual CTAB.[55] So modifying the AuNR surface

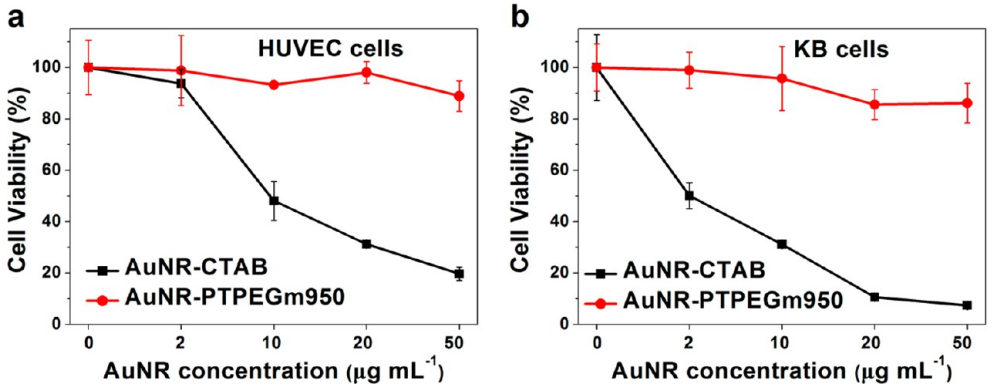

Figure 3. Cytotoxicity of (a) HUVEC cells and (b) KB cells evaluated by MTT assay after incubation with AuNR-CTAB and AuNR-PTPEGm950 with different Au concentrations for 24 h. Error bars represent the mean ± SD ($n \geq 3$).

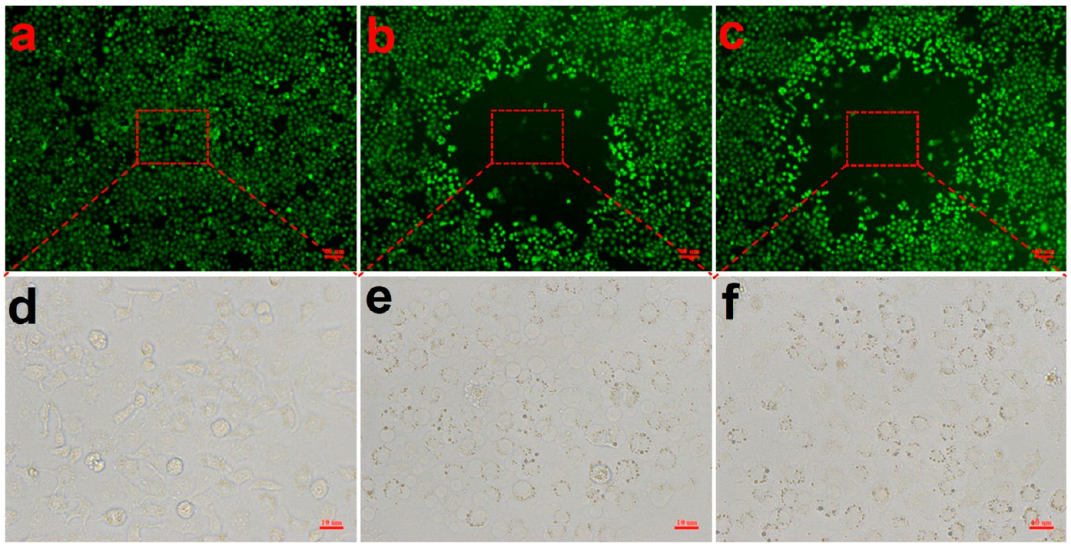

Figure 4. Cell viability of HepG2 cells was assessed via fluorescein diacetate (FDA) staining, after cell irradiation with 808 nm laser of 400 mW for 1 min in the presence of AuNRs at concentrations of (a) 0 μg mL^{-1}, (b) 25 μg mL^{-1}, and (c) 50 μg mL^{-1}. Scale bars in parts a–c are 40 μm. (d–f) Micrographs of cells at bright field corresponding to cells under laser irradiation at center of parts a–c. Scale bars in parts d–f are 10 μm.

with suitable ligands is important to improve their biocompatibility. Cytotoxicity of AuNP-PTPEGm950 was evaluated by both MTT assay compared with AuNR-CTAB (after three rounds of centrifugation) in both normal cell line human umbilical vein endothelial cell (HUVEC) and cancer cell line human oral epidermoid carcinoma cell (KB) (Figure 3). It was observed that the cytotoxicity of AuNR-CTAB on cancer KB cells was higher than that on normal HUVEC cells, which might result from many complicated factors depending on the cell types. It was also reported that the AuNR-CTAB exhibited selective toxicity to cancer cells rather than normal cells because of the different intracellular localization between normal and cancer cells.[56] After modification, the AuNR-PTPEGm950 showed no obvious cytotoxicity for both types of cells in all tested concentrations up to 50 μg mL^{-1} (gold atoms), while the AuNR-CTAB exhibited much higher cytotoxicity. These results demonstrated that modification with the multidentate PEG can greatly reduce the cytotoxicity of AuNRs, which promised their application in vivo.

3.4. NIR Photothermal Ablation of Cancer Cells in Vitro. The photothermal therapy effect of AuNR-PTPEGm950 was first evaluated in vitro, which was performed by directly irradiating the cancer cells with NIR laser after cell exposure to AuNR-contained medium. Cell viability of cells after treatment was assessed via fluorescein diacetate (FDA) staining, in which living cells can be stained to emit strong green fluorescence while damaged cell cannot be stained. Here, HepG2 cells were used because they have good adhesion ability on cell culture plate during the washing process after FDA staining, which reflects the actual photothermal effect of AuNRs on the treated cells. As shown in Figure 4a, after irradiation with a continuous wave (CW) diode laser of 808 nm with a ~1 mm focused spot size at power of 400 mW for 1 min, the cells without AuNRs kept good viability. Under the same irradiation, when the cells were incubated with AuNRs at a concentration of 25 μg mL^{-1}, an obvious dark spot appeared in the fluorescent image because of the photothermal damage of the cells (Figure 4b). The dark spot caused by the cell death under the laser center became larger as the concentration of AuNRs increased to 50 μg mL^{-1} (Figure 4c). With the same laser power, a higher concentration of AuNRs produced more heat which resulted in a larger damage spot of cells. The cell damage was caused by the hyperthermic effect generated from the AuNRs that absorbed the NIR laser radiation and converted it into local heating through nonradiative mechanisms,[30,57] which may result in a series of changes at the molecular level, including changes to

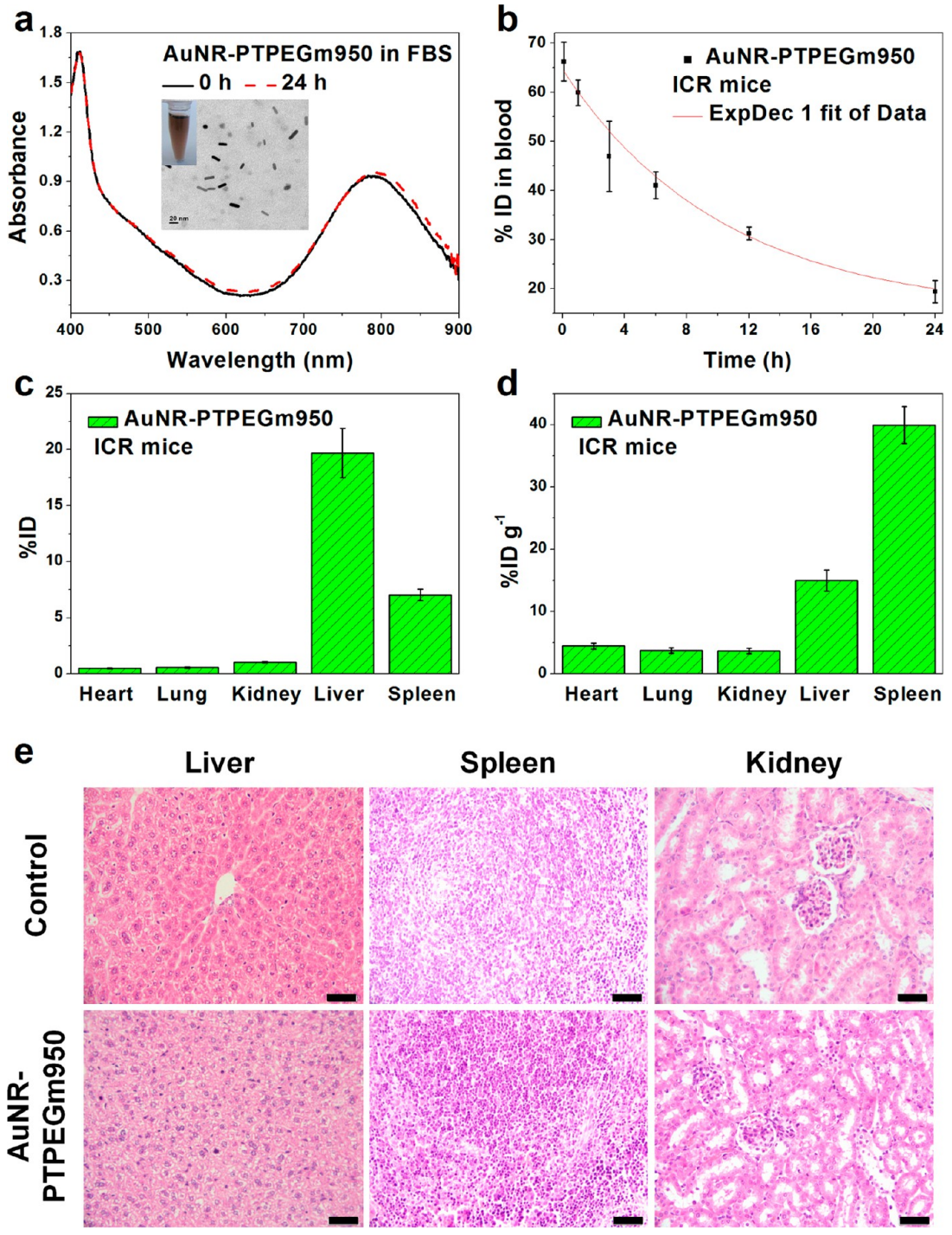

Figure 5. (a) UV−vis spectra of AuNR-PTPEGm950 after incubation in 100% FBS for 0 and 24 h. Insets: A solution of AuNRs incubated in FBS for 24 h and a TEM image of AuNRs dispersed in FBS. The blood circulation curve (b, the data fitted to monoexponential decay model) and biodistribution (c, given in % ID; d, given in % ID g^{-1}) at 24 h pi of AuNR-PTPEGm950 after intravenous injection in ICR mice. Error bars represent the mean ± SD (n = 3). (e) Representative H&E stained images of major organs including liver, spleen, and kidney collected from the control untreated mice and AuNP injected mice at 24 h postinjection in ICR mice. Scale bars in (e) are 20 μm. Here each mouse was injected at a single dose of 100 μg of AuNRs.

the cytoskeletal structure, cell membrane rupture, protein denaturation, impairment of DNA and RNA synthesis, and programmed apoptosis.[4] Figure 4d−f showed the morphology of the irradiated cells, where the changed cell morphology with blebbing of the cell membrane was observed for the cells with AuNRs (Figure 4e,f), while no visible change in cell morphology was observed for cells without AuNRs (Figure 4d). It indicated that the fast ablation of cancer cells was mainly caused by the heat induced destruction of the cell membrane.

3.5. Blood Circulation, Tissue Distribution, and Biocompatibility of AuNR-PTPEGm950. Before the study of photothermal therapy in vivo, we investigated the blood circulation and tissue distribution of multidentate PEG modified AuNRs. First, we tested the stability of AuNR-

dx.doi.org/10.1021/am5001823 | ACS Appl. Mater. Interfaces 2014, 6, 5657−5668

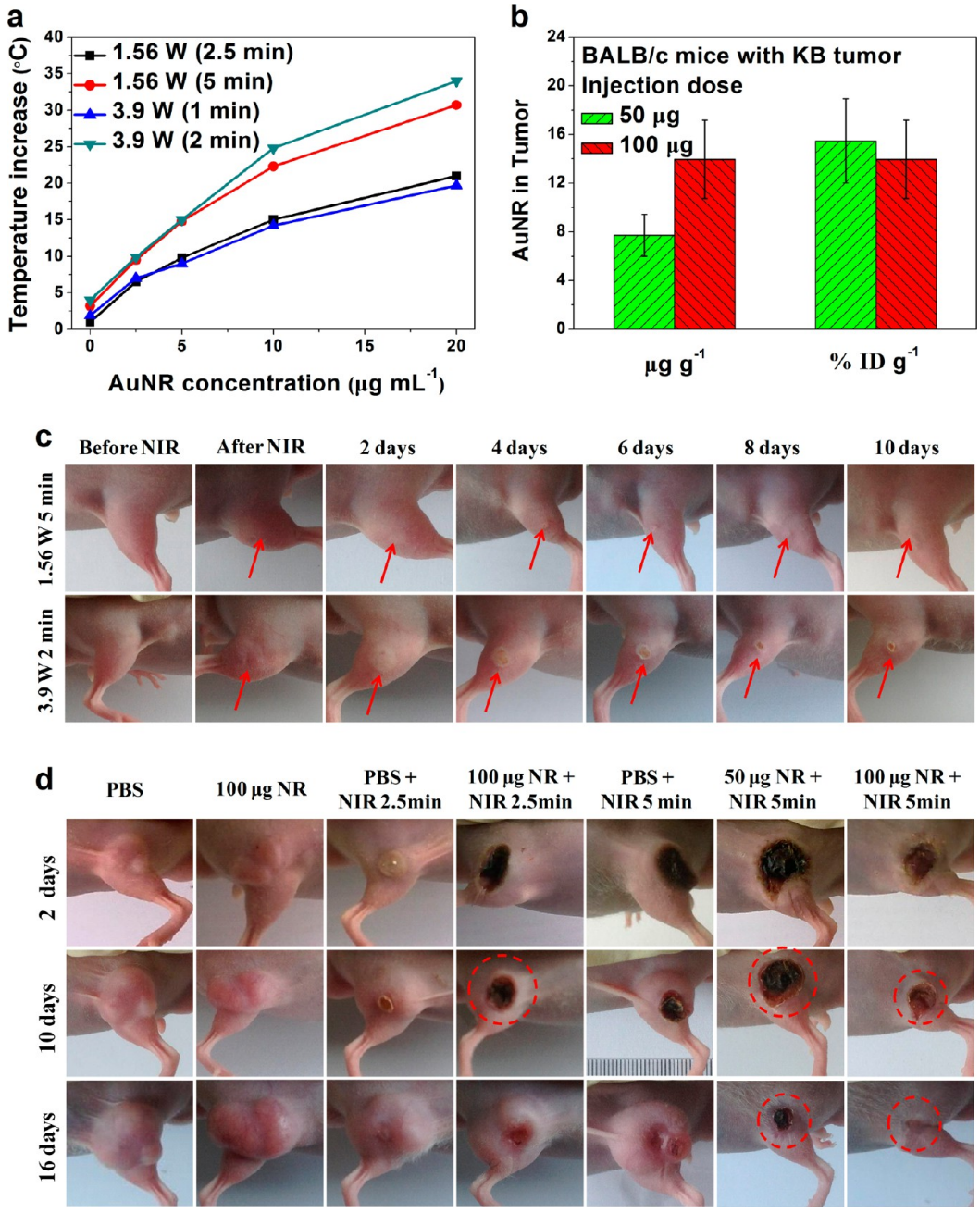

Figure 6. (a) Plots of temperature increase of PBS solutions with AuNR-PTPEGm950 after irradiation under different conditions versus the concentration of AuNRs. (b) Accumulation of AuNR-PTPEGm950 in tumors at 24 h pi with injection doses of 50 μg and 100 μg of Au per mouse (given in μg g^{-1} tumor and % ID g^{-1} tumor). Error bars represent the mean ± SD (n = 3). (c) Photothermal effect of NIR irradiation at different conditions on normal tissue without AuNRs. Representative digital photos of mouse thighs up to 10 days after irradiated at a power of 1.56 W for 5 min (upper row) and at a power of 3.9 W for 2 min (bottom row). Red arrows mark the irradiation sites. (d) Photothermal therapy of KB tumor-bearing mice by irradiating the tumors with NIR CW laser after a single injection of AuNR-PTPEGm950 for 24 h. Representative digital photos of tumors on mouse thigh up to 16 days after treatment with different therapeutic conditions. Red dotted circles mark the completely ablated tumors.

PTPEGm950 in serum. The absorption spectrum of AuNRs after incubation in 100% fetal bovine serum (FBS) for 24 h still kept a good shape without notable change (Figure 5a). No aggregation or sedimentation was observed for the solution of AuNRs in FBS, which kept a bright brown color (Figure 5a, inset digital image). The TEM image also showed the AuNR-PTPEGm950 well dispersed in the FBS (Figure 5a, inset TEM image). These results indicated that the multidentate PEG modified AuNRs had good stability in the biological condition. Next, we investigated the kinetics of AuNR circulation in the bloodstream after intravenously injecting AuNRs into ICR mice. The blood circulation curves of AuNR-PTPEGm950 is shown in Figure 2a (given in % of the injected dose (% ID)), and the experimental data can be fitted to a monoexponential decay model,[58] resulting in a half-decay time ($t_{1/2}$) of ~10.3 ± 2.4 h. It was also reported that the CTAB-stabilized AuNRs were rapidly cleared out from blood within 0.5 h after intravenous injection.[51] Here, the PTPEGm950 was proved to greatly prolong the blood circulation time of AuNRs which can be considered to possess long-circulating properties.[44,59] In

dx.doi.org/10.1021/am5001823 | ACS Appl. Mater. Interfaces 2014, 6, 5657−5668

this study, the used PTPEGm950 has a side chain of PEG with a molecular weight of 950 Da. For this type of polythiol PEG ligand, the PEG segments could be changed with different molecular weights, which with a higher molecular weight may bring a longer circulation time.[59] A thorough examination of how the multidentate PEG ligands designed with different molecular weights of PEG side chains impact blood circulation of the multidentate ligand modified NPs would be important and merits further investigation in future studies. It would make us understand better the difference between the multidentate PEG and monothiol-anchored PEG for nanoparticle modification. Figure 5c shows the biodistribution of AuNR-PTPEGm950 in main organs at 24 h postinjection, which showed that NRs accumulated in the liver and spleen with much higher quantity than in the heart, kidneys, and lung as expected because of the strong phagocytosis in RES organs. The highest accumulation of NPs was found in the liver (~20% ID), followed by the spleen (~8% ID). Considering that the spleen is much smaller than the liver, the concentration of AuNR-PTPEGm950 in spleen was much higher than that in liver (Figure 5d, ~40% ID g^{-1} vs ~15% ID g^{-1}).

Additionally, no apparent histopathological abnormalities or lesions were observed in liver, spleen, and kidney in the AuNR-PTPEGm950 treated mice by H&E staining, which showed no noticeable toxic effect of these multidentate PEGylated AuNRs on the major organs of mice at 24 h after administration (Figure 5e). Combined with the in vitro cytotoxicity results (Figure 3), these preliminarily results indicate ideal biocompatibility of the multidentate PEGylated AuNRs for in vivo applications.

3.6. NIR Photothermal Ablation of Tumors Mediated by AuNR-PTPEGm950. The hyperthermia of tumours is based on the phenomenon that most of tumors have a reduced tolerance for exposure to temperatures in the range 42−47°C compared to normal tissue, which is due to their poor blood supply.[30,57,60] To make sure that the photothermal effect of AuNRs can generate enough heat for tumor ablation, we investigated the temperature change of PBS solution with AuNR-PTPEGm950 as functions of AuNR concentration and laser power. As shown in Figure 6a, after irradiation, the temperatures of AuNR-PTPEGm950 PBS solution at a concentration of 20 μg mL^{-1} were increased by 21.0 °C at a power of 1.56 W for 2.5 min, 30.7 °C at a power of 1.56 W for 5 min, 19.7 °C at a power of 3.9 W for 1 min, and 34.0 °C at a power of 3.9 W for 2 min. In contrast, the temperature of pure PBS increased by less than 4 °C at the four types of irradiation. Considering that the in vivo temperature of the human body is ~37 °C, mediated with AuNRs and NIR irradiation, the tumor tissues can easily be heated to over 42 °C within a short time. At the same concentration of AuNRs, irradiation for a longer time resulted in a much higher temperature increase as expected. When the concentration of AuNRs is between 5 and 20 μg mL^{-1}, for different laser power, it was found that the temperature increase was slightly higher for 1.56 W for 2.5 min than that of 3.9 W for 1 min, while temperature increase for 3.9 W for 2 min was higher than that of 1.56 W for 5 min. It indicated that the irradiation with different laser power would result in a different temperature increase even if the laser energy is the same. No matter what kind of power, the temperature increased dramatically as the concentration of AuNRs increased. So a high accumulation of AuNRs in tumors should be crucial to the therapeutic effect.

The accumulation of AuNR-PTPEGm950 in xenografted KB tumors after intravenous injection for 24 h was evaluated at injection doses of 50 and 100 μg (Figure 6b). It showed that a higher injection dose resulted in a higher concentration of AuNRs in tumors, where the accumulation was ~7.7 μg g^{-1} tumor at a dose of 50 μg and ~13.9 μg g^{-1} tumor at a dose of 100 μg. Converting the data to % ID g^{-1}, the results were similar without significant difference, which were ~15.5% ID g^{-1} at a dose of 50 μg and ~13.9% ID g^{-1} at dose of 100 μg. The level of AuNRs in tumors could be considered as a high accumulation which is much higher than that in non-RES organs (Figure 5d, heart, lung, and kidney), and it is also comparable with that of the monothiol-anchored PEG5000 modified AuNRs.[44] It has been demonstrated that it needs to maintain a range 42−47 °C for tens of minutes to kill cancer cells; this duration can be shortened to only a few minutes for temperatures over 50 °C.[61,62] As estimated from the temperature increase in PBS solution (Figure 6a), after irradiation at a power of 1.56 W for 5 min, the temperature could increase ~18.8 °C with a tumor accumulation of ~7.7 μg g^{-1} and ~23.6 °C with a tumor accumulation of ~13.9 μg g^{-1}. The temperature increase would be higher if the irradiation was applied at a power of 3.9 W for 2 min. When these temperature enhancements were added to the body temperature (~37 °C), the tumor tissues can be heated to over 50 °C, enough to kill the cancer cells efficiently within minutes.

Although the NIR region is considered as a transparency window in the human body due to the minimal absorption of NIR light by tissues, in fact the NIR laser radiation cannot completely traverse the tissue without any influence at high power.[60] Therefore, the safety threshold laser energy should be confirmed to exclude side effects on normal tissues arising from the irradiation. For in vivo study, we first investigated the photothermal effect of NIR irradiation on normal tissues without AuNRs by irradiating the mouse thigh at a power of 1.56 W for 5 min or at a power of 3.9 W for 2 min by using an 808 nm CW laser with a focused spot size at ~6 mm. It showed that irradiation by laser at a power of 3.9 W for 2 min resulted in a big blister on the mouse thigh after 2 days and gradually developed into an eschar (Figure 6c, bottom row). In contrast, the injury to the tissue was negligible when irradiating by laser at a power of 1.56 W for 5 min (Figure 6c, upper row). The results indicated that a laser with too large a power will inevitably injure the normal tissue. Considering that the temperature increases of the AuNR solution were similar, generated by the two types of irradiation with the same energy, the laser power of 1.56 W for 5 min was chosen to be the maximum energy for the next in vivo ablation of tumors to avoid burning of the normal tissues.

The in vivo AuNR-mediated NIR photothermal therapy was performed using a KB tumor xenografts model. Nude mice bearing KB tumors were intravenously injected with AuNR-PTPEGm950 at different doses for 24 h and then subjected to a single 808 nm CW laser exposure at a power of 1.56 W for different times. Figure 6d presents the representative digital photos of tumors at times for the 2nd, 10th, and 16th day after different kinds of treatments. It showed that the control group with only AuNR injection but no laser irradiation had no influence on tumor growth (Figure 6d, the second column). The control group without AuNRs but treated with a low laser energy irradiation of 1.56 W for 2.5 min caused a blister on the 2nd day, which then developed into an eschar on the grown tumor on the 10th day (Figure 6d, the 3rd column). Similarly,

the control group without AuNRs but treated with a high laser energy irradiation of 1.56 W for 5 min showed a more serious injury to the tumors, which caused big black scars on the tumors on the 2nd day after treatment (Figure 6d, the 5th column). These results showed that the NIR laser irradiation is more destructive to tumor tissue than to normal tissues because the tumors have a reduced tolerance for hyperthermia.[30,57,60] However, the NIR laser irradiation with this energy cannot completely suppress the growth of tumors. The tumors treated by irradiation of 1.56 W for 2.5 min grew as big as tumors in the control group without irradiation at the 16th day. Obvious reoccurrence of the tumors treated by irradiation of 1.56 W for 5 min happened around the black scars on the 10th day (the tumors started to relapse on the 4th to 6th days) and the tumors reconstructed with big sizes on the 16th day. For the treatment group with an intravenous injection of AuNR-PTPEGm950 at a dose of 100 μg and irradiation of 1.56 W for 2.5 min, although the tumors were reconstructed on the 16th day, the growth of tumors was almost suppressed up to the 10th day, which was much better than the control group with the same irradiation conditions (Figure 6d, the 4th column). When the irradiation time was prolonged to 5 min, the treatment group with an injection dose of 100 μg of AuNRs still showed a very effective therapeutic effect (Figure 6d, the 7th column). In this group, the tumors were ablated completely without showing reoccurrence even after 40 days, and the scars of tumors fell off and normal healthy skin reconstructed. Even in the treatment group with irradiation of 1.56 W for 5 min and a low dose of 50 μg of AuNRs, the tumors did not recur during the following 16 days and the scars on the thigh gradually became smaller and smaller (Figure 6d, the 6th column). Although a statistical information (volume of tumors) of tumor ablation would be helpful to evaluate the photothermal therapeutic effect, here we did not provide the volume growth curves of tumors because tumors ablated form scars that make the volume measurements not exact. For example, the tumors in the groups (Figure 6b; the 4th column, 100 μg of NR + NIR 2.5 min; the 4th column, PBS + NIR 5 min) first form scars and later recurred around the scars but left a scar hole in the recurred tumors, which makes it difficult to measure their exact volumes. These successful tumor photothermal therapeutic effects were attributed to the generation of local heat from the accumulated AuNRs in the tumor site under sufficient laser irradiation which is high enough for complete destruction of tumor tissue. The results demonstrated that the multidentate PEG modified AuNRs can serve as an effective photothermal agent for tumor ablation by a single intravenous administration and one-time NIR laser irradiation of safe energy to normal tissues.

When using AuNRs as photothermal agent for cancer therapy, the question of whether the AuNRs are still stable after near-infrared irradiation is always raised. Although some references reported that the AuNRs would melt after irradiation with high laser energy,[62] our results showed that the PEGylated AuNRs were quite stable after five runs of irradiation with a 808 nm laser of 1.56 W for 5 min which is strong enough to completely ablate tumors in this study (Figure S2). So the AuNRs are suitable to serve as a photothermal agent for in vivo photothermal therapy of tumors. We believe that based on this study, further designed multidentate ligands that make modified AuNRs with higher tumor accumulation will be beneficial for obtaining effective therapy by a lower NIR laser energy in the future.

4. CONCLUSION

In summary, we demonstrated that the multidentate PEG ligand modified AuNRs can serve as an effective NIR photothermal agent for tumor ablation in vivo. A type of multidentate ligand of polythiol PEG-based copolymer was used to successfully stabilize AuNRs in solutions with high saline concentration and wide pH range. The multidentate PEG greatly increased the ligand affinity to the AuNR core, which showed much stronger resistance to the DTT competition than monothiol-anchored PEG ligand did. After surface modification, the cytotoxicity of AuNRs was remarkably reduced compared to that of the original CTAB coated ones, and the PEGylated AuNRs had low toxicity on main organs of mice in vivo. The AuNR-PTPEGm950 showed high efficacy for the ablation of cancer cells in vitro, where cells were killed easily by irradiating with a NIR laser in the presence of AuNRs but there was no damage on cells when in absence of AuNRs. Moreover, the AuNR-PTPEGm950 showed good stability in serum, and they had a long circulation time in blood and led to a high accumulation in tumors. Importantly, tumors irradiated by NIR 808 nm laser with a suitable energy after intravenous injection of AuNR-PTPEGm950 could be completely ablated, form eschars without reoccurrence, and finally reconstruct with normal tissues. These encouraging results suggest that AuNR-PTPEGm950 has great potential in serving as an effective photothermal agent for future clinical cancer therapy. It also strongly indicates that the multidentate PEG surfaces could be widely used to stabilize various NPs and successfully deliver them to disease sites, which is important for realizing the fascinating functions of NPs for biomedical applications in vivo.

■ ASSOCIATED CONTENT

Ⓢ Supporting Information

Figure S1showing stabilities of AuNR-CTAB and Figure S2 showing photostability of AuNRs after near-infrared irradiation. This material is available free of charge via the Internet at http://pubs.acs.org.

■ AUTHOR INFORMATION

Corresponding Author

*E-mail: jijian@zju.edu.cn. Tel/Fax: (+86)-571-87953729.

Notes

The authors declare no competing financial interest.

■ ACKNOWLEDGMENTS

Financial support from Grants NSFC-21174126 and 51333005, National Science Fund for Distinguished Young Scholars (Grant 51025312), the National Basic Research Program of China (Grant 2011CB606203) and Research Fund for the Doctoral Program of Higher Education of China (Grants 20110101110037, 20110101120049, and 20120101130013), and Open Project of State Key Laboratory of Supramolecular Structure and Materials (Grant sklssm201316) are gratefully acknowledged. We thank Guping Tang and Jun Zhou for animal experiments, Ying Xu and Hua Wang for TEM analyses, and Zigang Xu for ICP-MS analyses.

■ REFERENCES

(1) Boisselier, E.; Astruc, D. Gold Nanoparticles in Nanomedicine: Preparations, Imaging, Diagnostics, Therapies and Toxicity. *Chem. Soc. Rev.* **2009**, *38*, 1759−1782.

(2) Huang, H.-C.; Barua, S.; Sharma, G.; Dey, S. K.; Rege, K. Inorganic Nanoparticles for Cancer Imaging and Therapy. *J. Controlled Release* **2011**, *155*, 344−357.
(3) Dreaden, E. C.; Mackey, M. A.; Huang, X. H.; Kang, B.; El-Sayed, M. A. Beating Cancer in Multiple Ways Using Nanogold. *Chem. Soc. Rev.* **2011**, *40*, 3391−3404.
(4) Kennedy, L. C.; Bickford, L. R.; Lewinski, N. A.; Coughlin, A. J.; Hu, Y.; Day, E. S.; West, J. L.; Drezek, R. A. A New Era for Cancer Treatment: Gold-Nanoparticle-Mediated Thermal Therapies. *Small* **2011**, *7*, 169−183.
(5) Lohse, S. E.; Murphy, C. J. Applications of Colloidal Inorganic Nanoparticles: From Medicine to Energy. *J. Am. Chem. Soc.* **2012**, *134*, 15607−15620.
(6) Ang, L. Y.; Lim, M. E.; Ong, L. C.; Zhang, Y. Applications of Upconversion Nanoparticles in Imaging, Detection and Therapy. *Nanomedicine* **2011**, *6*, 1273−1288.
(7) Jain, R. K.; Stylianopoulos, T. Delivering Nanomedicine to Solid Tumors. *Nat. Rev. Clin. Oncol.* **2010**, *7*, 653−664.
(8) Duan, X.; Li, Y. Physicochemical Characteristics of Nanoparticles Affect Circulation, Biodistribution, Cellular Internalization, and Trafficking. *Small* **2013**, *9*, 1521−1532.
(9) Maeda, H.; Wu, J.; Sawa, T.; Matsumura, Y.; Hori, K. Tumor Vascular Permeability and the EPR Effect in Macromolecular Therapeutics: A Review. *J. Controlled Release* **2000**, *65*, 271−284.
(10) Moghimi, S. M.; Hunter, A. C.; Murray, J. C. Long-Circulating and Target-Specific Nanoparticles: Theory to Practice. *Pharmacol. Rev.* **2001**, *53*, 283−318.
(11) Li, S.-D.; Huang, L. Pharmacokinetics and Biodistribution of Nanoparticles. *Mol. Pharmaceutics* **2008**, *5*, 496−504.
(12) Dobrovolskaia, M. A.; Aggarwal, P.; Hall, J. B.; McNeil, S. E. Preclinical Studies To Understand Nanoparticle Interaction with the Immune System and Its Potential Effects on Nanoparticle Biodistribution. *Mol. Pharmaceutics* **2008**, *5*, 487−495.
(13) Verma, A.; Stellacci, F. Effect of Surface Properties on Nanoparticle−Cell Interactions. *Small* **2010**, *6*, 12−21.
(14) Erathodiyil, N.; Ying, J. Y. Functionalization of Inorganic Nanoparticles for Bioimaging Applications. *Acc. Chem. Res.* **2011**, *44*, 925−935.
(15) Gong, Y.; Winnik, F. M. Strategies in Biomimetic Surface Engineering of Nanoparticles for Biomedical Applications. *Nanoscale* **2012**, *4*, 360−368.
(16) Quarta, A.; Curcio, A.; Kakwere, H.; Pellegrino, T. Polymer Coated Inorganic Nanoparticles: Tailoring the Nanocrystal Surface for Designing Nanoprobes with Biological Implications. *Nanoscale* **2012**, *4*, 3319−3334.
(17) Nandanan, E.; Jana, N. R.; Ying, J. Y. Functionalization of Gold Nanospheres and Nanorods by Chitosan Oligosaccharide Derivatives. *Adv. Mater.* **2008**, *20*, 2068−2073.
(18) Smith, A. M.; Nie, S. Minimizing the Hydrodynamic Size of Quantum Dots with Multifunctional Multidentate Polymer Ligands. *J. Am. Chem. Soc.* **2008**, *130*, 11278−11279.
(19) Liu, L.; Guo, X.; Li, Y.; Zhong, X. Bifunctional Multidentate Ligand Modified Highly Stable Water-Soluble Quantum Dots. *Inorg. Chem.* **2010**, *49*, 3768−3775.
(20) Stewart, M. H.; Susumu, K.; Mei, B. C.; Medintz, I. L.; Delehanty, J. B.; Blanco-Canosa, J. B.; Dawson, P. E.; Mattoussi, H. Multidentate Poly(ethylene glycol) Ligands Provide Colloidal Stability to Semiconductor and Metallic Nanocrystals in Extreme Conditions. *J. Am. Chem. Soc.* **2010**, *132*, 9804−9813.
(21) Na, H. B.; Palui, G.; Rosenberg, J. T.; Ji, X.; Grant, S. C.; Mattoussi, H. Multidentate Catechol-Based Polyethylene Glycol Oligomers Provide Enhanced Stability and Biocompatibility to Iron Oxide Nanoparticles. *ACS Nano* **2012**, *6*, 389−399.
(22) Chen, X.; Lawrence, J.; Parelkar, S.; Emrick, T. Novel Zwitterionic Copolymers with Dihydrolipoic Acid: Synthesis and Preparation of Nonfouling Nanorods. *Macromolecules* **2013**, *46*, 119−127.
(23) Giovanelli, E.; Muro, E.; Sitbon, G.; Hanafi, M.; Pons, T.; Dubertret, B.; Lequeux, N. Highly Enhanced Affinity of Multidentate versus Bidentate Zwitterionic Ligands for Long-Term Quantum Dot Bio-Imaging. *Langmuir* **2012**, *28*, 15177−15184.
(24) Palui, G.; Na, H. B.; Mattoussi, H. Poly(ethylene glycol)-Based Multidentate Oligomers for Biocompatible Semiconductor and Gold Nanocrystals. *Langmuir* **2012**, *28*, 2761−2772.
(25) Liu, X.; Huang, H.; Liu, G.; Zhou, W.; Chen, Y.; Jin, Q.; Ji, J. Multidentate Zwitterionic Chitosan Oligosaccharide Modified Gold Nanoparticles: Stability, Biocompatibility and Cell Interactions. *Nanoscale* **2013**, *5*, 3982−3991.
(26) Gravel, E.; Tanguy, C.; Cassette, E.; Pons, T.; Knittel, F.; Bernards, N.; Garofalakis, A.; Ducongé, F.; Dubertret, B.; Doris, E. Compact Tridentate Ligands for Enhanced Aqueous Stability of Quantum Dots and in Vivo Imaging. *Chem. Sci.* **2013**, *4*, 411−417.
(27) Liu, X.; Huang, N.; Wang, H.; Li, H.; Jin, Q.; Ji, J. The Effect of Ligand Composition on the in Vivo Fate of Multidentate Poly (Ethylene Glycol) Modified Gold Nanoparticles. *Biomaterials* **2013**, *34*, 8370−8381.
(28) Zhan, N.; Palui, G.; Safi, M.; Ji, X.; Mattoussi, H. Multidentate Zwitterionic Ligands Provide Compact and Highly Biocompatible Quantum Dots. *J. Am. Chem. Soc.* **2013**, *135*, 13786−13795.
(29) Huang, X.; Jain, P. K.; El-Sayed, I. H.; El-Sayed, M. A. Gold Nanoparticles: Interesting Optical Properties and Recent Applications in Cancer Diagnostics and Therapy. *Nanomedicine* **2007**, *2*, 681−693.
(30) Huang, X.; Jain, P. K.; El-Sayed, I. H.; El-Sayed, M. A. Plasmonic Photothermal Therapy (PPTT) Using Gold Nanoparticles. *Lasers Med. Sci.* **2008**, *23*, 217−228.
(31) Choi, W. I.; Kim, J. Y.; Kang, C.; Byeon, C. C.; Kim, Y. H.; Tae, G. Tumor Regression in Vivo by Photothermal Therapy Based on Gold-Nanorod-Loaded, Functional Nanocarriers. *ACS Nano* **2011**, *5*, 1995−2003.
(32) Weissleder, R. A Clearer Vision for in Vivo Imaging. *Nat. Biotechnol.* **2001**, *19*, 316−317.
(33) Lal, S.; Clare, S. E.; Halas, N. J. Nanoshell-Enabled Photothermal Cancer Therapy: Impending Clinical Impact. *Acc. Chem. Res.* **2008**, *41*, 1842−1851.
(34) Huang, X. H.; Neretina, S.; El-Sayed, M. A. Gold Nanorods: From Synthesis and Properties to Biological and Biomedical Applications. *Adv. Mater.* **2009**, *21*, 4880−4910.
(35) Skrabalak, S. E.; Chen, J.; Sun, Y.; Lu, X.; Au, L.; Cobley, C. M.; Xia, Y. Gold Nanocages: Synthesis, Properties, and Applications. *Acc. Chem. Res.* **2008**, *41*, 1587−1595.
(36) Melancon, M. P.; Lu, W.; Yang, Z.; Zhang, R.; Cheng, Z.; Elliot, A. M.; Stafford, J.; Olson, T.; Zhang, J. Z.; Li, C. In Vitro and in Vivo Targeting of Hollow Gold Nanoshells Directed at Epidermal Growth Factor Receptor for Photothermal Ablation Therapy. *Mol. Cancer Ther.* **2008**, *7*, 1730−1739.
(37) Ma, Y.; Liang, X.; Tong, S.; Bao, G.; Ren, Q.; Dai, Z. Gold Nanoshell Nanomicelles for Potential Magnetic Resonance Imaging, Light-Triggered Drug Release, and Photothermal Therapy. *Adv. Funct. Mater.* **2013**, *23*, 815−822.
(38) Alkilany, A. M.; Thompson, L. B.; Boulos, S. P.; Sisco, P. N.; Murphy, C. J. Gold Nanorods: Their Potential for Photothermal Therapeutics and Drug Delivery, Tempered by the Complexity of Their Biological Interactions. *Adv. Drug Delivery Rev.* **2012**, *64*, 190−199.
(39) Chen, H.; Shao, L.; Li, Q.; Wang, J. Gold Nanorods and Their Plasmonic Properties. *Chem. Soc. Rev.* **2013**, *42*, 2679−2724.
(40) Huang, X.; El-Sayed, I. H.; Qian, W.; El-Sayed, M. A. Cancer Cell Imaging and Photothermal Therapy in the Near-Infrared Region by Using Gold Nanorods. *J. Am. Chem. Soc.* **2006**, *128*, 2115−2120.
(41) Huff, T. B.; Tong, L.; Zhao, Y.; Hansen, M. N.; Cheng, J.-X.; Wei, A. Hyperthermic Effects of Gold Nanorods on Tumor Cells. *Nanomedicine* **2007**, *2*, 125−132.
(42) Zhou, W.; Shao, J.; Jin, Q.; Wei, Q.; Tang, J.; Ji, J. Zwitterionic Phosphorylcholine as a Better Ligand for Gold Nanorods Cell Uptake and Selective Photothermal Ablation of Cancer Cells. *Chem. Commun.* **2010**, *46*, 1479−1481.
(43) Dickerson, E. B.; Dreaden, E. C.; Huang, X.; El-Sayed, I. H.; Chu, H.; Pushpanketh, S.; McDonald, J. F.; El-Sayed, M. A. Gold

Nanorod Assisted Near-Infrared Plasmonic Photothermal Therapy (PPTT) of Squamous Cell Carcinoma in Mice. *Cancer Lett.* **2008**, *269*, 57−66.
(44) von Maltzahn, G.; Park, J. H.; Agrawal, A.; Bandaru, N. K.; Das, S. K.; Sailor, M. J.; Bhatia, S. N. Computationally Guided Photothermal Tumor Therapy Using Long-Circulating Gold Nanorod Antennas. *Cancer Res.* **2009**, *69*, 3892−3900.
(45) Chen, R.; Zheng, X.; Qian, H.; Wang, X.; Wang, J.; Jiang, X. Combined Near-IR Photothermal Therapy and Chemotherapy Using Gold-Nanorod/Chitosan Hybrid Nanospheres To Enhance the Antitumor Effect. *Biomater. Sci.* **2013**, *1*, 285−293.
(46) Ren, F.; Bhana, S.; Norman, D. D.; Johnson, J.; Xu, L.; Baker, D. L.; Parrill, A. L.; Huang, X. Gold Nanorods Carrying Paclitaxel for Photothermal-Chemotherapy of Cancer. *Bioconjugate Chem.* **2013**, *24*, 376−386.
(47) Chen, R.; Wang, X.; Yao, X.; Zheng, X.; Wang, J.; Jiang, X. Near-IR-Triggered Photothermal/Photodynamic Dual-Modality Therapy System via Chitosan Hybrid Nanospheres. *Biomaterials* **2013**, *34*, 8314−8322.
(48) von Maltzahn, G.; Centrone, A.; Park, J. H.; Ramanathan, R.; Sailor, M. J.; Hatton, T. A.; Bhatia, S. N. SERS-Coded Gold Nanorods as a Multifunctional Platform for Densely Multiplexed Near-Infrared Imaging and Photothermal Heating. *Adv. Mater.* **2009**, *21*, 3175−3180.
(49) Jokerst, J. V.; Cole, A. J.; Van de Sompel, D.; Gambhir, S. S. Gold Nanorods for Ovarian Cancer Detection with Photoacoustic Imaging and Resection Guidance via Raman Imaging in Living Mice. *ACS Nano* **2012**, *6*, 10366−10377.
(50) Alkilany, A. M.; Murphy, C. J. Toxicity and Cellular Uptake of Gold Nanoparticles: What We Have Learned So Far? *J. Nanopart. Res.* **2010**, *12*, 2313−2333.
(51) Niidome, T.; Yamagata, M.; Okamoto, Y.; Akiyama, Y.; Takahashi, H.; Kawano, T.; Katayama, Y.; Niidome, Y. PEG-Modified Gold Nanorods with a Stealth Character for in Vivo Applications. *J. Controlled Release* **2006**, *114*, 343−347.
(52) Nikoobakht, B.; El-Sayed, M. A. Preparation and Growth Mechanism of Gold Nanorods (NRs) Using Seed-Mediated Growth Method. *Chem. Mater.* **2003**, *15*, 1957−1962.
(53) Murphy, C. J.; Sau, T. K.; Gole, A. M.; Orendorff, C. J.; Gao, J.; Gou, L.; Hunyadi, S. E.; Li, T. Anisotropic Metal Nanoparticles: Synthesis, Assembly, and Optical Applications. *J. Phys. Chem. B* **2005**, *109*, 13857−13870.
(54) Khanal, B. P.; Zubarev, E. R. Rings of Nanorods. *Angew. Chem., Int. Ed.* **2007**, *46*, 2195−2198.
(55) Alkilany, A. M.; Nagaria, P. K.; Hexel, C. R.; Shaw, T. J.; Murphy, C. J.; Wyatt, M. D. Cellular Uptake and Cytotoxicity of Gold Nanorods: Molecular Origin of Cytotoxicity and Surface Effects. *Small* **2009**, *5*, 701−708.
(56) Wang, L.; Liu, Y.; Li, W.; Jiang, X.; Ji, Y.; Wu, X.; Xu, L.; Qiu, Y.; Zhao, K.; Wei, T. Selective Targeting of Gold Nanorods at the Mitochondria of Cancer Cells: Implications for Cancer Therapy. *Nano Lett.* **2010**, *11*, 772−780.
(57) Chatterjee, D. K.; Diagaradjane, P.; Krishnan, S. Nanoparticle-Mediated Hyperthermia in Cancer Therapy. *Ther. Delivery* **2011**, *2*, 1001−1014.
(58) Shin, D. M.; Huang, X. H.; Peng, X. H.; Wang, Y. Q.; Wang, Y. X.; El-Sayed, M. A.; Nie, S. M. A Reexamination of Active and Passive Tumor Targeting by Using Rod-Shaped Gold Nanocrystals and Covalently Conjugated Peptide Ligands. *ACS Nano* **2010**, *4*, 5887−5896.
(59) Chan, W. C. W.; Perrault, S. D.; Walkey, C.; Jennings, T.; Fischer, H. C. Mediating Tumor Targeting Efficiency of Nanoparticles Through Design. *Nano Lett.* **2009**, *9*, 1909−1915.
(60) Svaasand, L. O.; Gomer, C. J.; Morinelli, E. On the Physical Rationale of Laser Induced Hyperthermia. *Lasers Med. Sci.* **1990**, *5*, 121−128.
(61) Habash, R. W.; Bansal, R.; Krewski, D.; Alhafid, H. T. Thermal Therapy, Part 1: An Introduction to Thermal Therapy. *Crit. Rev. Biomed. Eng.* **2006**, *34*, 459−489.
(62) Liu, Y.; Ai, K.; Liu, J.; Deng, M.; He, Y.; Lu, L. Dopamine−Melanin Colloidal Nanospheres: An Efficient Near-Infrared Photothermal Therapeutic Agent for in Vivo Cancer Therapy. *Adv. Mater.* **2013**, *25*, 1353−1359.